


The Differentiation of Soft Tissue Infiltration and Surrounding Edema in an Animal Model of Malignant Bone Tumor: Evaluation by Dual-Energy CT

Technology in Cancer Research & Treatment
Volume 18: 1-5
© The Author(s) 2019
Article reuse guidelines:
sagepub.com/journals-permissions
DOI: 10.1177/1533033819846842
journals.sagepub.com/home/tct


Haisong Chen, PhD, MD¹ , Yuan Zhang, MD¹, Jing Pang, MD¹,
Zengjie Wu, MD¹, Meng Jia, MD¹, Qian Dong, PhD, MD¹,
and Wenjian Xu, PhD, MD¹ 

Abstract

To study the value of dual energy computed tomography in distinguishing soft tissue infiltration from surrounding soft tissue edema in rabbit malignant bone tumor, a malignant bone tumor model was established through implantation of VX2 tumor fragments into the tibiae of rabbits. Tumor adjacent soft tissues were divided into 3 areas according to pathology and computed tomography images. Computed tomography spectral curve slopes and iodine and water concentrations were assessed. Statistical analyses were performed using the Mann-Whitney *U* test and *t* test. The spectral curve of the soft tissue infiltration areas has a slope (1.30 ± 0.41) higher than that of the soft tissue edema areas (0.71 ± 0.23 ; $P < .001$). The iodine concentration in the soft tissue infiltration areas (8.56 ± 2.15) was higher than that in the soft tissue edema areas (6.09 ± 1.02 ; $P < .001$). Water concentration was similar in the soft tissue infiltration areas (1033.86 ± 10.50) to that of the edema areas (1031.45 ± 12.83 ; $P < .05$). Spectral curve analysis and iodine–water concentration are helpful in the differentiation of bone tumor soft tissue infiltration and soft tissue edema.

Keywords

bone neoplasm, malignant, edema, dual energy CT

Abbreviations

CNR, contrast–noise ratio; CT, computed tomography; DECT, dual-energy CT; MRI, magnetic resonance imaging; ROI, region of interests

Received: September 18, 2018; Revised: November 3, 2018; Accepted: March 21, 2019.

Introduction

Differentiating soft tissue infiltration from surrounding edema is important for the precise resection of bone tumors; however, this is difficult to achieve using conventional computed tomography (CT). Human tissues cannot be reliably distinguished by conventional CT, because the hybrid attenuation over the whole energy scope, rather than a specific energy, is measured.^{1,2} Positron emission tomography/CT is limited by its low resolution for the definition of lesion margins. Dynamic contrast-enhanced magnetic resonance imaging (MRI) has the ability to distinguish between the two because tumor tissues are enhanced in the early stages after injection of contrast medium, whereas edema is

enhanced in the late stages.³ However, in some cases, the edema area is enhanced early because of the rapid uptake of contrast material by slow-flowing capillaries inside the surrounding soft tissue edema.⁴ Therefore, new imaging modalities are needed.

¹ Department of Radiology, the Affiliated Hospital of Qingdao University, Qingdao, China

Corresponding Author:

Wenjian Xu, PhD, MD, Department of Radiology, the Affiliated Hospital of Qingdao University, Qingdao, China.
Email: cjr.xuwenjian@vip.163.com



Substances with markedly different attenuation spectra can be differentiated by dual-energy CT (DECT).⁵ It has been proved that every substance has its own specific X-ray spectral curve. So, if the X-ray spectral curve of a tissue is obtained, the contents inside the tissue can be acknowledged. Double kVP technique of DECT can generate a series of virtual CT images under different single-energy X-ray and spectral curves of any region of interests (ROIs) and thus can differentiate the gradients of the substance scanned.⁶ The X-ray absorption of any tissues can be expressed by that of 2 basic substances with different X-ray attenuation such as iodine and water, which were most common pair of combination being used, for the couple covers the attenuation of most gradients of medical imaging from soft tissue to iodine contrast medium. With the water and iodine as the pair of basic substance, the accurate CT values of tissues under different mono-energy rather than average CT value under hybrid energy can be obtained by the 2 groups of data under 2 different kVP.⁷ The measurement of iodine concentration on iodine basic image and water concentration on water basic image could also be valuable in distinguishing contents of lesions.⁸

In a previous study from our group,⁹ we studied intramedullary infiltration of bone tumor in a VX2 rabbit model. However, whether DECT can differentiate soft tissue invasion from soft tissue edema and normal muscle remains unclear. The objective of the present study was to assess DECT findings in the rabbit VX2 tumor model of a larger sample of 50 rabbits to study whether the spectral curve can accurately differentiate soft tissue invasion from soft tissue edema and normal muscle and to assess differences in iodine and water concentrations among the abovementioned 3 areas.

Materials and Methods

Animals

The ethnical committee of our hospital where the study took place approved this study. The rabbit VX2 carcinoma models were established as described in our previous study.⁹ The tumor was cut from the tumor-bearing rabbits and smashed into small fragments and implanted into the right proximal tibia of healthy rabbits with electrical drill and forceps. Ketamine with a dose of 1.6 mL/kg was injected into rabbit thigh muscles before the implantation. Two weeks after the implantation, ultrasound examination was performed to confirm the tumor formation. Fifty VX2 carcinoma rabbit models with weight from 2 to 3 kg were successfully made.

Spectral CT Examinations

Spectral CT was performed 1 month after implantation of the tumor. The study was performed using a 128-slice DECT of 1 X-ray tube with transient exchanging between 2 different voltage of 140 KV and 80 KV (Discovery CT750 HD; GE Healthcare, Milwaukee, Wisconsin). After scan, the data were transferred automatically to the workstation of the scanner.

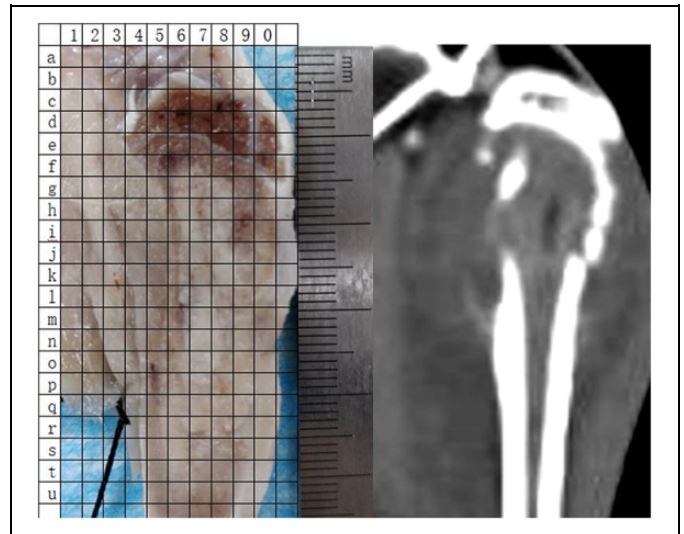


Figure 1. The rabbit calve was cut down and cross-sectioned into sagittal 2-mm-thick slices, and the largest section (the left figure) was used to compare with that of the monochromatic image of computed tomography (CT; the right figure).

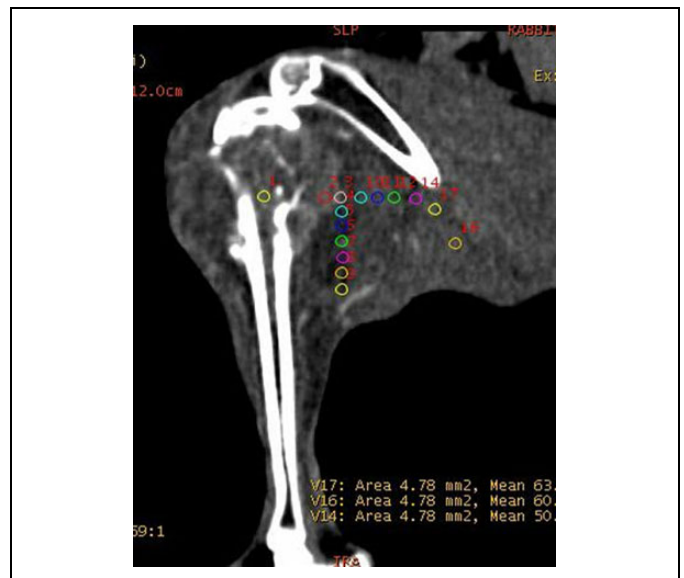


Figure 2. Monochromatic sagittal multiplanar reconstruction (MPR)-enhanced image of the tibia at 140 keV and the positions of region of interests (ROIs). The ROIs cover the soft tissue infiltration area, edema area, and normal muscle area. The soft tissue infiltration area manifested as an area of obviously computed tomography (CT)-enhanced soft tissue mass with tumor cells inside the mass under microscopy. However, the area of edema and normal muscle area cannot be distinguished on CT images.

An X-ray attenuation curve (spectral curve) was automatically generated by placing the ROIs on a solid component in the soft tissue lesions without necrosis and hemorrhage (Figures 1 and 2).

The examinations included plain and dynamic-enhanced DECT scan. The parameters of scan are as follows: current of X-ray tube, 400 mA and slice thickness 1-mm pitch of scan,

0.5. The dynamic-enhanced DECT scanning was performed with bolus injection of nonionic contrast material (300 mgI/mL, 2.0 mL/kg) with a flow rate of 2.0 mL/s into the rabbit ear vein, and the scanning started at 10, 20, 30, 60 and 120 seconds from the beginning of the injection. Sagittal reconstruction-enhanced CT image with single energy of 140 keV, where the highest contrast–noise ratio (CNR) was shown on the CNR curve, was used to be compared with pathological specimen.

Histopathological Examinations

After CT examinations, air was injected intravenously into the ears of rabbits to kill them and then the rabbits were preserved in a refrigerator at a temperature of -80°C . Three days later, the rabbit calves including the knee and ankle joint were cut down and cross-sectioned into sagittal 2-mm-thick slices, and the largest section was used to compare with that of the monochromatic image of CT (Figure 1). Then, the specimen was separated into squares with an edge length of 2 cm to match the size of the glass slide. Tissue sections were then numbered and photographed (for dot to dot comparison with CT images) and sent to the department of pathology to do paraffin embedding and pathological staining with hematoxylin and eosin and observed under microscope.

Pathology and CT Analysis

According to the pathological sections of the tibia, their appearance under a microscope (Figure 3A and B), and the sagittal reconstruction-enhanced CT images, the soft tissues adjacent to the bone tumor were divided into 3 areas as follows: area A was defined as the soft tissue infiltration of the tumor and manifested as an area of obviously enhanced soft tissue mass with tumor cells inside the mass under microscopy; area B was the peripheral soft tissue edema area without tumor cells, but may there be a few inflammatory cells inside this area; and area C consisted of the normal muscle without edema or tumor cell inside.

Two senior radiologists reviewed the images of CT for the shapes of the spectral curves (the differences of the slopes), and the concentrations of iodine and water in the 3 areas were defined by pathological results and compared to corresponding CT images. Both radiologists reviewed and defined ROIs in all animals in consensus. Three to 5 consecutive ROIs with a diameter of 2 mm were delineated in each of the above 3 areas, keeping away from nonenhancing areas such as tumor bone and necrosis. The curves of the energy spectrum and their slopes were formed and calculated automatically by software. The slope $k = (\text{HU}40 \text{ keV} - \text{HU}100 \text{ keV})/60$, where Hu40 keV and Hu100 keV represented the CT values of the ROI at 40 keV and 100 keV, respectively. Iodine/water concentrations were also measured automatically.

Statistical Analysis

One-way variance analysis and Mann-Whitney U test were used, respectively, to compare the differences in spectral curve

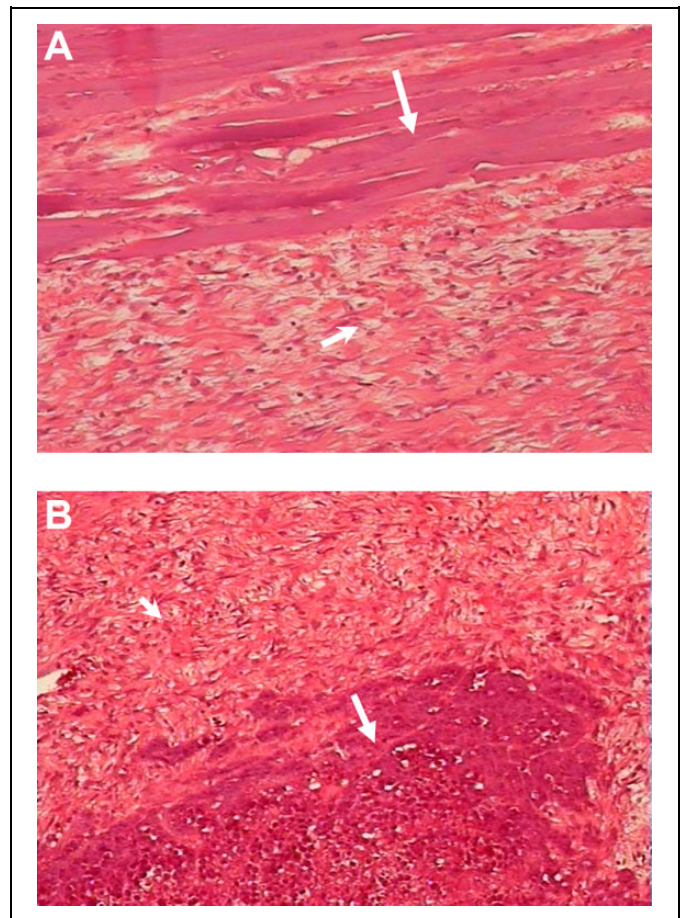


Figure 3. A, Pathological slice (HE $\times 10$) showing the soft tissue invasion area with tumor cells in a tile arrangement (long arrow) and the edema area (short arrow). The margin between the 2 areas is clear. B, Pathological slice (HE $\times 10$) showing the edema area (short arrow) and normal muscle (long arrow). The margin between the 2 areas is clear. HE indicates hematoxylin and eosin.

slopes and the concentrations of iodine and water between the 3 groups. Bilateral P values $< .05$ were thought to be significance.

Results

Successful modeling was achieved in all 50 rabbits, which was confirmed by histopathologic results. For the spectral curves of ROIs in the soft tissue edema areas, their slopes (0.71 ± 0.23) were significantly smaller than that in the soft tissue infiltration areas (1.30 ± 0.41 ; $P < .05$) and greater than that in normal muscles (0.35 ± 0.12 ; $P < 0.01$; Figure 4).

The iodine concentration in the soft tissue edema areas ($6.09 \pm 1.02 \text{ g/L}$) was lower than that in the soft tissue infiltration areas ($8.56 \pm 2.15 \text{ g/L}$; $P < .05$) and higher than that in normal muscles ($2.72 \pm 0.43 \text{ g/L}$; $P < .001$).

The water concentration of normal muscles ($1047.47 \pm 10.97 \text{ g/L}$) was larger than that in the soft tissue infiltration areas ($1033.21 \pm 10.50 \text{ g/L}$) and soft tissue edema areas ($1033.12 \pm 12.83 \text{ g/L}$; $P < .05$), although the difference between the latter two did not reach statistical significance ($P > .05$).

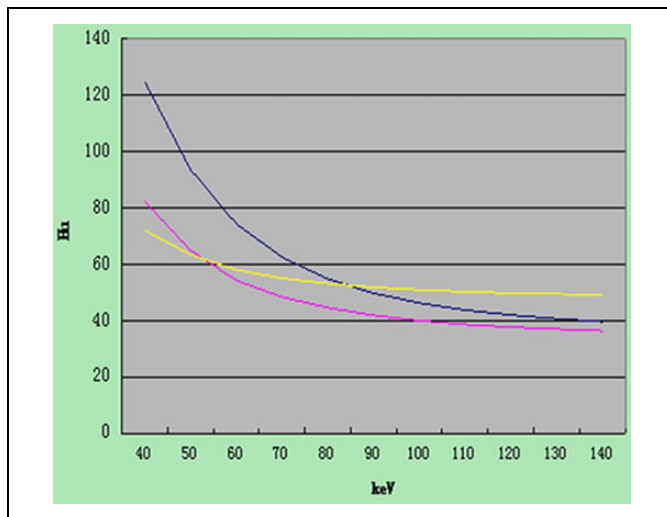


Figure 4. An example of the spectral curves of 3 region of interests (ROIs) in the area of soft tissue infiltration, edema, and normal muscle, respectively, of a single animal. The slope of the spectral curve in the soft tissue edema area was significantly greater than that in the normal muscle and smaller than that in the soft tissue infiltration area. Pink curve: one of the curves of the ROIs in edema area. Yellow curve: one of the curves of the ROIs in normal muscle area. Blue curve: one of the curves of the ROIs in soft tissue infiltration area.

Discussion

Spectral Curves of Soft Tissue Invasion From Bone Tumors

X-ray attenuation curves (spectral curves) can reflect the characteristics of the different tissues because of the ability of DECT to display their virtual hounsfield units (Hus) (instead of hybrid CT values). The soft tissue invasion area is the result of the expansion of the bone tumor into the soft tissue, and it consists of tumor cells (together with some necrotic and hemorrhagic areas, which are excluded from the regions of study). We examined the spectral curves of the soft tissue invasion of VX2 bone tumors and found differences among the slopes of the curves of tumors, edema areas, and normal muscles, possibly due to differences in cell type, distribution pattern, metabolism, and blood supply. The curve slope of the soft tissue infiltration areas (1.30 ± 0.41) was proved to be significantly greater than that of the soft tissue edema areas (0.71 ± 0.23) and normal muscles (0.35 ± 0.12) in this study. The degree of attenuation differed among the 3 areas, especially in the part of low energy, possibly due to the low penetration of X-ray and high tissue contrast at the low energy level. This result is similar to the report of Coursey *et al.*¹⁰ which showed the CT values of the spectral curve vary greatly in the low energy range. Therefore, a low energy range (eg, 40-100 keV) should be chosen to analyze the images and accurately show the differences in the slopes.¹¹

Iodine and Water Concentration of Soft Tissue Invasion of Bone Tumor

In the areas of soft tissue extension from hypervascular bone tumors, the iodine deposition can be shown on iodine-based images with high sensitivity. The exact reason for the differences in iodine concentration among the 3 regions is unknown; however, possible explanations include formation of tumor vessels and the high permeability in tumor areas of richer capillary than in edema areas and healthy muscles that result in more leaking of contrast agent of iodine. Thus, the concentration of iodine reflects the amounts or density and immaturity of abnormal vessel in the tumor areas. As shown in our study, the iodine concentration in the soft tissue infiltration areas (8.56 ± 2.15 g/L) was higher than that in soft tissue edema areas (6.09 ± 1.02 g/L) and normal muscles (2.72 ± 0.43 g/L).

The water concentration in the soft tissue infiltration areas (1033.21 ± 10.50) was lower than that in normal muscles (1047.47 ± 10.97); this may be caused by a decrease in free water due to the narrowing space between the cells as a result of a high multiplication rate and tight arrangement, but this hypothesis needs further validation using diffusion-weighted MRI. The water concentration in soft tissue edema areas (1033.12 ± 12.83) were lower than that in normal muscles (1047.47 ± 10.97), which could be a consequence of the narrowing space between swelling cells.

Shortcomings in This Study

Although differences were shown in the slopes of the curves and iodine/water concentrations between the soft tissue invasion areas and surrounding edema areas, we did not provide details on how to define the borders between the 2 areas. Second, the sample size is small (50). Hence, further study is needed.

Conclusions

The soft tissue invasion of malignant bone tumor can be distinguished from soft tissue edema and normal muscle by spectral CT in the rabbit model.

Authors' Note

The ethical committee of our hospital where the study took place approved this study. The Animal Care and Use Committee of the Affiliated Hospital of Qingdao University approved the experimental procedures (approval no. QDFYKYLL-2018-10-15). All animal housing and experiments were conducted in strict accordance with the institutional Guidelines for Care and Use of Laboratory Animals. The data sets used and/or analyzed during the current study are available from the corresponding author on reasonable request. This article had been presented in World Congress and Expo on Oncology & Radiology.

Acknowledgments

We would like to thank Prof. Zhang Guixiang and Li Kangan from the Department of Radiology, the Affiliated First People's Hospital of

Shanghai Jiaotong University for providing tumor cell strain and technical support.

Declaration of Conflicting Interests


The author(s) declared no potential conflicts of interest with respect to the research, authorship, and/or publication of this article.

Funding

The author(s) disclosed receipt of the following financial support for the research, authorship, and/or publication of this article: This work was supported by the National Natural Science Foundation of China [grant numbers 81571673, 81671658].

ORCID iD

Haisong Chen, PhD, MD  <https://orcid.org/0000-0002-4746-5193>

Wenjian Xu, PhD, MD  <https://orcid.org/0000-0002-5106-6953>

References

1. Ohira S, Karino T, Ueda Y, et al. How well does dual-energy CT with fast kilovoltage switching quantify CT number and iodine and calcium concentrations? *Acad Radiol*. 2018;25(4):519-528.
2. Ramon A, Bohm-Sigraund A, Pottecher P, et al. Role of dual-energy CT in the diagnosis and follow-up of gout: systematic analysis of the literature. *Clin Rheumatol*. 2018;37(3):587-595.
3. Andrea BM. Malignant versus benign vertebral collapse: are new imaging techniques useful?. *Cancer Imaging*. 2009;9(Special issue A):S49-S51.
4. Gaeta M, Benedetto C, Minutoli F, et al. Use of diffusion-weighted, intravoxel incoherent motion, and dynamic contrast enhanced MR imaging in the assessment of response to radiotherapy of lytic bone metastases from breast cancer. *Acad Radiol*. 2014;21(10):1286-1293.
5. Pessis E, Campagna R, Sverzut JM, et al. Virtual monochromatic spectral imaging with fast kilovoltage switching: reduction of metal artifacts at CT. *Radiographics*. 2013;33(2):573-583.
6. Thomas C, Schabel C, Krauss B, et al. Dual-energy CT: virtual calcium subtraction for assessment of bone marrow involvement of the spine in multiple myeloma. *AJR Am J Roentgenol*. 2015;204(3):W324-W331.
7. Nicolaou S, Liang T, Murphy DT, Korzan JR, Ouellette H, Munk P. Dual-energy CT: a promising new technique for assessment of the musculoskeletal system. *Am J Roentgenol*. 2012;199(5):S78-S86.
8. Lv P, Lin XZ, Li J, Li W, Chen K. Differentiation of small hepatic hemangioma from small hepatocellular carcinoma: recently introduced spectral CT method. *Radiology*. 2011;259(3):720-729.
9. Chen H, Jia M, Xu W. Malignant bone tumor intramedullary invasion: evaluation with dual-energy computed tomography in a rabbit model. *J Comput Assist Tomogr*. 2015;39(1):70-74.
10. Coursey CA, Nelson RC, Boll DT, et al. Dual-energy multidetector CT: how does it work, what can it tell us, and when can we use it in abdominopelvic imaging? *Radiographics*. 2010;30(4):1037-1055.
11. Shi JW, Dai HZ, Shen L, Xu DF. Dual-energy CT: clinical application in differentiating an adrenal adenoma from a metastasis. *Acta Radiol*. 2014;55(4):505-512.